铝合金 LB-RSW 焊接中 RSW 温度场的数值模拟

李永强[1], 赵 贺[2], 赵熹华[1], 蒋文虎[3], 张伟华[1]

(1. 吉林大学 材料科学与工程学院, 长春 130022;
2. 哈尔滨工业大学 现代焊接生产技术国家重点试验室, 哈尔滨 150001;
3. 第一汽车集团公司 技术中心, 长春 130011)

摘 要: 使用 Ansys 软件进行了"激光束—电阻缝焊"(LB-RSW)中电阻缝焊(RSW)过程的热结构和热电的循环顺序分析, 研究了缝焊电流、焊接速度和滚盘间距对铝板 RSW 温度场的影响. 结果表明, 铝板表面温度及滚盘前、后方的温度梯度随着缝焊电流的增加而升高或增大, 温度的最高值与缝焊电流的平方近似成正比关系; 铝板表面温度随着 RSW 速度的升高而降低, 升降温速度随着焊接速度的增加而增大; 铝板表面的最高温度随着滚盘间距的增加而降低, 滚盘后方的温度梯度随着滚盘间距的增加而减小. 模拟结果与热成像照片吻合良好, 为预测激光与电阻热源复合最佳匹配位置和 LB-RSW 机理研究奠定了基础.

关键词: 电阻缝焊; 激光焊; 温度场; 数值模拟
中图分类号: TG402 文献标识码: A 文章编号: 0253—360X(2009)04—0029—04

李永强

0 序 言

"激光束—电阻缝焊"(LB-RSW, 国际发明专利号: PCT/WO2007008363A2)是一种崭新的复合焊接方法[1,2], 其激光焊缝是在电阻缝焊(RSW)的加压、加热和强电磁场辅助作用下形成的. 电阻热—机械(力)作用可以起到提高金属材料对激光的吸收率[3]、降低所需激光功率及减少热裂纹和接头残余应力等显著效果. 所以深入研究 RSW 的温度场对于预测激光与电阻热源复合最佳匹配位置和 LB-RSW 的机理都十分重要. 虽然国内外在电阻点焊和凸焊的数值模拟方面做了大量的工作[4—6], 但电阻缝焊方面的研究尚鲜见报道.

使用 Ansys 有限元分析软件, 对搭接铝合金 LB-RSW 焊接中 RSW 温度场进行数值分析, 并用红外热像仪的测量结果验证模拟的可靠性.

1 有限元模型和边界条件

1.1 有限元模型

LB-RSW 焊接过程如图 1 所示, 焊接时工件匀速运动, 滚盘电极压紧在工件上, 旋转并通电, 焊缝由激光和电阻热复合热源共同形成.

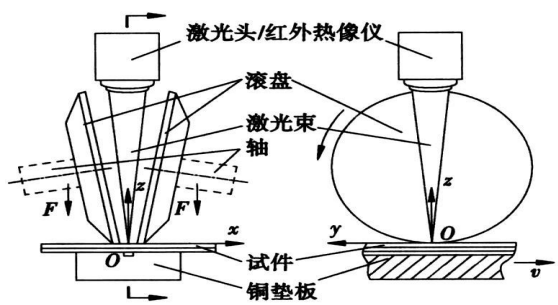

图 1 LB-RSW 焊接示意图

Fig. 1 Schematic of LB-RSW experimental apparatus

滚盘、铝试件和铜垫板的几何模型由 Pro/E 生成, 通过图形接口导入 Ansys 软件. 试件为 114 mm × 40 mm × 2 mm 的 5182 铝合金板, 铜垫板上开有 5 mm 宽、3.75 mm 深的焊漏槽, 滚盘与工件接触处厚度为 4.2 mm, RSW 变压器次级分别与两滚盘电极相连, 电流的主要流动方向垂直于焊缝.

由于 RSW 几何模型空间上的复杂性和对称性, 取其 1/2 建立面对称 3D 有限元模型, 并把模型中温度、应力和电场变化较大区域的网格划分得较密, 如

收稿日期: 2008—12—24
基金项目: 国家自然科学基金资助项目(50575091)

图2 所示(图 2 的坐标系与图 1 相同). 结构分析时选用 Solid45 单元, 电热分析时选用 Solid69 单元.

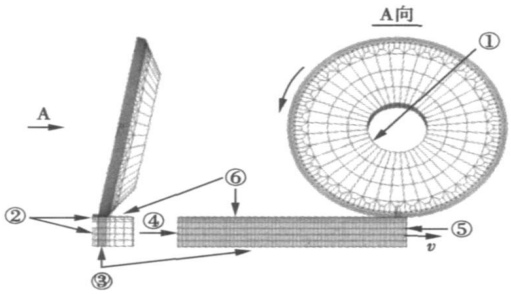

图 2 三维 RSW 过程有限元模型

Fig. 2 Finite element model of 3D RSW process

1.2 对滚盘和工件运动的处理

对工件的运动处理方式如图3 所示, 其中 $t_{1-0}=t_2-t_1=t_3-t_2=t_4-t_3=t_5-t_4=t_6-t_5=t_7-t_6=t_8-t_7=\triangle t$, $s_{1-0}=s_2-s_1=s_3-s_2=s_4-s_3=s_5-s_4=\triangle s$. 假设焊接时工件匀速运动, 则工件的实际位移如图 3 中虚线所示, 图中当 $0<t<t_1$ 和 $t_7<t<t_8$ 时工件静止, $t_1<t<t_7$ 时工件匀速运动; 模拟中工件的运动是步进的, 即工件在 t_2, t_3, t_4, t_5, t_6, t_7 等时间点上移动, 其它时间保持静止; 对滚盘的转动也使用同样的处理方法. 可知 $\triangle t$ 越小, 对工件和滚盘运动的处理越接近实际情况. 文中所用的 $\triangle t\leqslant 0.047$ s, 此时 $\triangle t$ 对温度场的影响已经很小.

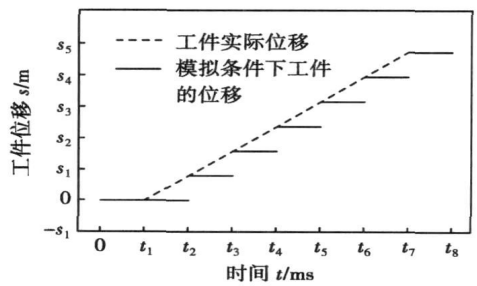

图 3 模拟中对工件移动的处理

Fig. 3 Solution method on workpiece motion in numerical simulation

做如下简化和假设: 材料力学性能采用拉压同性材料模式, 材料硬化模式为各向同性, 采用 Von Misses 屈服准则; 交流电流简化为等效的直流电流, 不考虑电流趋表效应; 忽略接触热阻; 辐射和热对流用综合换热系数代替.

1.3 多物理场耦合模拟流程

缝焊过程涉及结构、电、热等的多场耦合, 使用 Ansys 软件的 APDL 语言编制的程序流程如图 4 所示. (1) 在预压阶段, 通过结构分析得到在电极压力的作用下电极—铝板和铝板—铝板间的接触区域压力分布; (2) 在热电耦合分析中利用结构分析所得结果调整各个接触电阻单元的电阻率, 并得到这一载荷步结束时模型各节点的温度; (3) 移动工件, 旋转滚盘; (4) 在新模型中加载热电耦合分析得到的温度数据, 进行热结构耦合分析, 并得到新的接触区域和压力分布; (5) 不断重复 (2) ~ (4), 直至缝焊过程结束.

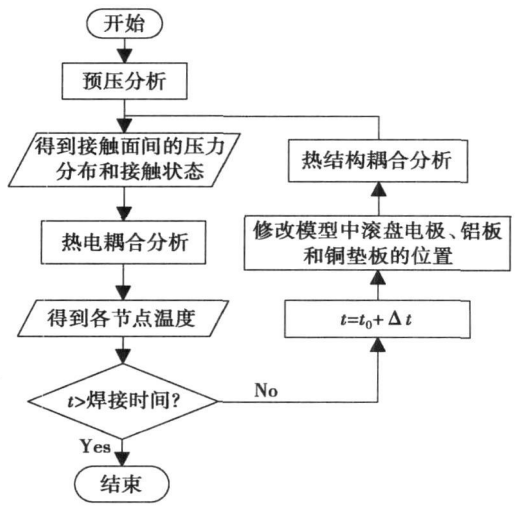

图 4 有限元分析流程图

Fig. 4 Flow chart of finite element analysis

1.4 边界条件

在热结构分析时, 耦合边界①上所有节点 x 轴和 y 轴方向上的自由度, 并施加电极压力; 在滚盘与上铝板氧化膜间、上铝板与下铝板氧化膜间和下铝板氧化膜与铜垫板间建立接触单元; 约束边界②上所有节点 x 轴方向上的自由度; 约束边界③所有节点 x 轴、y 轴和 z 轴方向上自由度; 约束边界④上所有节点 y 轴方向上的自由度; 除预压分析外对所有节点施加热电耦合分析得到的节点温度载荷.

在热电分析时, 耦合边界①上所有节点的电压, 并施加电流; 根据热弹性分析结果设置各个接触电阻单元的电阻率, 耦合接触区域对应节点的电压; 耦合铝板、铜垫板接触面上的对应节点的温度; 耦合边界②上所有节点的电压; 在边界④、边界⑤、边界⑥和滚盘表面施加热对流载荷.

1.5 接触电阻和材料性能参数

通过在铝板表面设置一层极薄的实体单元, 并

设置其电阻率来模拟接触电阻产热. 接触电阻与压强的关系如下式[5]，即

$$\rho_c(p)=69.489p^{-\frac{2}{3}}-3.501p^{-\frac{1}{2}}+0.051\,7^{-\frac{1}{3}} \quad (1)$$

$$\rho_{ew}(p)=3.851p^{-\frac{2}{3}}-0.162p^{-\frac{1}{2}}+0.002\,5^{-\frac{1}{3}} \quad (2)$$

式中：$\rho_c(p)$，$\rho_{ew}(p)$分别为工件间的接触电阻率和电极与工件间的接触电阻率；p 为接触压力.

综合考虑压力与温度对接触电阻的影响，文中的接触电阻率如下式，即

$$\rho_c(p,T)=\begin{cases}\rho_c(p)\cdot\dfrac{T_m-T}{T_m-T_0}+\rho(T), & T\leqslant T_m\\ \rho(T), & T>T_m\end{cases} \quad (3)$$

$$\rho_{ew}(p,T)=\begin{cases}\rho_{ew}(p)\cdot\dfrac{T_m-T}{T_m-T_0}+\rho(T), & T\leqslant T_m\\ \rho(T), & T>T_m\end{cases} \quad (4)$$

式中：$\rho_c(p,T)$和 $\rho_{ew}(p,T)$是综合考虑压力与温度后的接触电阻率；T_m 为铝合金熔点；T_0 为室温；T 为铝合金的温度；$\rho(T)$为铝合金的电阻率.

铝合金热物理性能参数见文献[5] 和文献[7]；滚盘电极和铜垫板的热物理性能见文献[8].

2　模拟结果及讨论

2.1　模拟结果

由于 LB-RSW 焊接时激光头的中心位于两滚盘的对称面上，所以着重研究了铝板上表面 y 轴上的温度（以下简称铝板表面温度）分布情况. 图 5、图 6 和图 7 的数据是工件在不同 RSW 参数下沿 y 轴负方向运动了 81 mm 时刻的值.

图 5 为缝焊电流对铝板表面温度影响. 从图 5a 中可以看出铝板表面温度随着 RSW 电流 I 的增加而大幅度升高，并且滚盘前、后方的温度梯度皆随着 I 的增加而增大. 在 $v=0.8$ m/min，$I=10$ kA 和滚盘间距 $d_1=5$ mm 时的最高温度达到了 352 ℃，这可为激光焊接提供足够高的预热温度. 从图 5b 可以看出其它参数固定的情况下铝板表面温度的最高值与 I^2 近似成正比关系.

图 6a 为不同焊接速度下铝板表面的温度分布. 从图中可以看出铝板表面温度随着 RSW 速度 v 的增加而降低，并且滚盘前、后方的温度梯度皆随着 v 的增加而增大；图 6b 为铝板上表面 y 轴与边界④距离为 85.9 mm 的点在不同焊接速度下的热循环曲线. 从图中可以看出铝板表面的升、降温速度都随着焊接速度的增加而提高.

图7为不同滚盘间距铝板表面温度分布. 从图

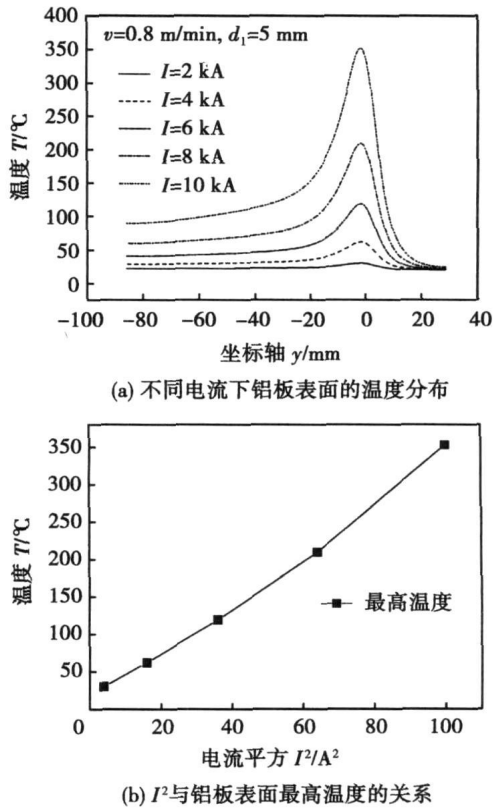

图 5　缝焊电流对温度的影响

Fig. 5　Effect of RSW current on temperature

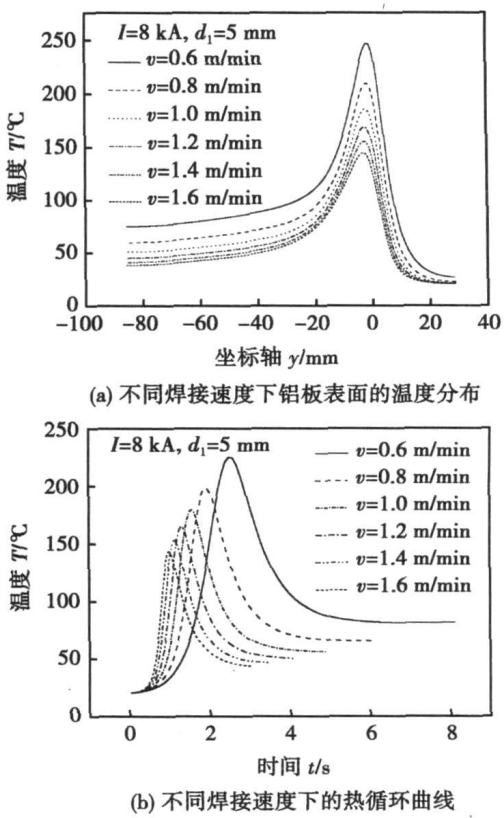

图 6　焊接速度对温度的影响

Fig. 6　Effect of RSW speed on temperature

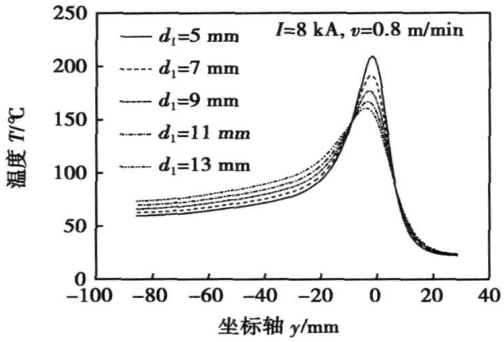

图 7 不同滚盘间距铝板表面的温度分布

Fig. 7 Temperature profile of surface of aluminum alloy plate under different RSW wheels spacing

中可以看出铝板表面温度随着滚盘间距的增加而降低，并且滚盘后方铝板的温度梯度随着 d_1 的增加而减小.

2.2 模拟结果的验证

使用 FLIR 公司的 ThermaCAM P20 红外热像仪对 RSW 的温度场进行了测量(图 1). 图 8 为 v=0.8 m/min, I=8 kA 和 d_1=5 mm 条件下模拟温度场与实拍温度场的对比. 需要说明的是，由于取景条件的限制，热成像照片的视野要比模拟结果的视野小很多(图中温度较低的部分为被遮挡住的部分). 从图中可以看出模拟所得的温度场与实测的温度场吻合良好，证明所采用的模拟方法是可靠的.

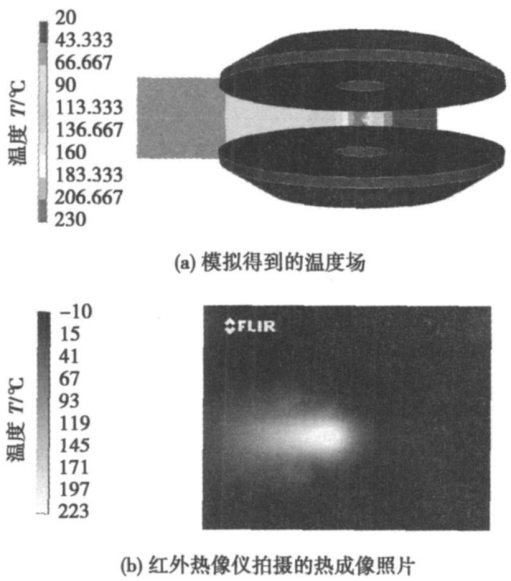

图 8 热成像照片与模拟结果对比

Fig. 8 Comparison between infrared thermography photo and numerical simulation result

3 结 论

(1) 使用 Ansys 软件对 LB-RSW 复合焊接中 RSW 的温度场进行了数值分析，研究了 RSW 中电流、速度和滚盘间距对温度场的影响，并通过热成像技术验证了模拟结果的可靠性.

(2) 铝板表面温度和滚盘前、后方的温度梯度随着 RSW 电流 I 的增加而升高或增大，并且铝板表面温度的最高值与 I^2 近似成正比关系.

(3) 铝板表面温度随着 RSW 速度的增加而降低，并且铝板表面的升降温速度随着焊接速度的增加而增大.

(4) 铝板表面的最高温度随着滚盘电极间距 d_1 的增加而降低，并且滚盘后方的温度梯度随着 d_1 的增加而减小.

致谢： 感谢哈尔滨焊接研究所在试验设备及人员上给予的支持和帮助.

参考文献：

[1] 赵熹华，曹海鹏，赵 贺，等. 激光束—电阻缝焊复合焊接方法基础研究[C] // 第十一次全国焊接会议论文集. 哈尔滨：黑龙江人民出版社，2005：388—390.

[2] Li Y Q, Zhao X H, Zhao H, *et al*. Study on the effect of welding current during laser beam-resistance seam welding of aluminum alloy 5052 [J]. China Welding, 2008, 17(2): 42—46.

[3] 左铁钏. 高强铝合金的激光加工[M]. 北京：国防工业出版社，2002.

[4] Song Q, Zhang W, Bay N. Contact modelling in resistance welding. part 1: algorithms and numerical verification[J]. Proceedings of the Institution of Mechanical Engineers, Part B: Journal of Engineering Manufacture, 2006, 220(5): 599—606.

[5] 杨黎峰. 铝合金电阻点焊熔核形成过程的数值模拟[D]. 长春：吉林大学，2005.

[6] 吴志生，杨新华，单 平，等. 铝合金点焊电极端面温度数值模拟[J]. 焊接学报，2004，25(6)：15—18.
Wu Zhisheng, Yang Xinhua, Shan Ping, *et al*. Numerical simulation of electrode tip temperature for spot welding aluminum alloy [J]. Transactions of the China Welding Institution, 2004, 25(6): 15—18.

[7] Mondolfo L F. Aluminum alloys: structure and properties[M]. London: Butterworth's Limited Company, 1976.

[8] West E G. 铜和铜合金[M]. 陈北盈，涂远军，孙啸华，译. 长沙：中南工业大学出版社，1987.

作者简介：李永强，男，1978 年出生，博士研究生. 主要研究方向为激光焊和压力焊. 发表论文 5 篇.

Email: zhaoxh@jlu.edu.cn

212013, Jiangsu, China; 2. Institute of Welding Engineering, Shanghai Jiao Tong University, Shanghai 200030, China). p17—20

Abstract: The recognition and positioning of start welding position (SWP) is the first step to realize intelligent robot welding. The definition of SWP is given based on the analysis of seam type. The macro-scopical images of workpieces to be welded are snapped by CCD camera in a relativly large range without additional light. The recognizing methods of SWP are analyzed according to its definition. A two-step method that from coarse to fine is proposed to recognize the SWP accurately. The first step is to solve the curve functions of seam and workpieces boundaries by fitting, and their intersection points are regarded as the initial value of SWP. The second step is to establish a small window that takes the initial values as the centre. And the SWP becomes exact by the corner detection in the window. Both the abundant information of original images and the structured information of recognized images are used according to the given judge rules, which take full advantage of the image information and improve the recognized precision. The detected results show that the actual position of SWP and recognized initial value by the first step are identical for the normal seam, but the recognized result by the first step is different from the actual position for the un-normal curve seam. The exact results can be obtained by the presented two-step method for both normal and un-normal curve seams.

Key words: start welding position; image recognition; are welding robot

Cracking control technology of TiC/Ni coatings prepared by in-situ fabrication through laser cladding HE Qingkun, WANG Yong, ZHAO Weimin, CHENG Yiyuan (Material Department, College of Mechanical and Electronic Engineering, China Petroleum University, Dongying 257061, Shandong, China). p21—24

Abstract: There are many cracks in TiC/Ni coatings prepared by in-situ fabrication through laser cladding. The reasons for crack initiation in the coatings were analyzed from the microstructure, the phase composition, the residual stress, the macro morphology and the fracture observation. Corresponding cracking control measures were also proposed. The investigation indicated that the cracks of the TiC/Ni coatings are mainly brittle cold cracks caused by hard brittle phases and internal residual stress. The replacement reaction ($M_{23}C_6+Ti\rightarrow M+TiC$) occurs by increasing the content of Ti powder. Therefore, cracks of the coatings can be reduced or eliminated. Moreover, intriguing microstructures of the coatings are obtained with enhanced plasticity and toughness and reduced residual stress by nickel powder addtion or by optimizing processing parameters, thus the cracking susceptibility can be decreased.

Key words: in-situ fabrication; laser cladding; cracking control; replacement reaction

Welding distortion prediction and control of thin-plate welded structures of the truck side-walls LI Yana, ZHAO Wenzhong, LU Bihong, NIE Chunge (School of Traffic Transportation, Dalian Jiaotong University, Dalian 116028, Liaoning, China). p25—28

Abstract: During the process of the truck side-walls welding, buckling deformation is caused by the shrinkage force in the weld seams. It is difficult to predict and control the distortion. The buckling deformation which not only reduces the strength but also affects the smoothness and the beauty of thin-plate. The welding distortion of the truck side-wall was studied using inherent strain as an equivalent load. The results show that the predicted results is consistent with the measured data. Based on the simulation model, the different factors involved in the design and welding affecting the distortion were investigated using the orthogonal design. The optimal design is presented, which provides reliable theoretical references for thin-plate welding deformation controlling of the truck side-walls.

Key words: thin-plate welded structure; welding distortion; inherent strain; orthogonal design

Numerical simulation of RSW temperature field during aluminum alloys LB-RSW LI Yongqiang[1], Zhao He[2], Zhao Xihua[1], Jiang Wenhu[3], Zhang Weihua[1] (1. School of Materials Science and Engineering, Jilin University, Changchun 130022, China; 2. State Key Laboratory of Advanced Welding Production Technology, Harbin Institute of Technology, Harbin 150001, China; 3. R & D center, FAW, Changchun 130011, China). p29—32

Abstract: The thermo-structural and thermo-electrical circular order analyses of resistance seam welding (RSW) process in laser beam-resistance seam welding (LB-RSW) were carried out by means of ANSYS, and the influences of RSW current, welding speed and the space between two RSW wheels on temperature field in RSW were studied. The results indicate the surface temperature of aluminum alloy plates and the temperature gradients both in front and back of wheels increase consequently with RSW current increasing. Meanwhile, the maximum temperature value presents direct ratio relationship with the square of current approximately. The surface temperature of aluminum alloy plates reduces with the increase of welding speed. However, the rate of temperature change appears a converse tendency when the welding speed increases. Besides, the maximum surface temperature of aluminum alloys plates decreases with the decrease of the space between two RSW wheels. Furthermore, the temperature gradient behind the RSW wheels also decreases when the space between the two wheels decrease. The simulation results match well with the thermography acquired by infrared thermography technology, which makes it feasible to predict the optimal relative position between laser beam and resistance heat source and to investigate the mechanism of LB-RSW.

Key words: resistance seam welding; laser welding; temperature field; numerical simulation

Temperature field simulation of electron beam rapid prototyping CHEN Yunxia, ZHU Miaofeng, LU Fenggui, YAO Shun (Welding Engineering Institute, Shanghai Jiaotong University, Shanghai 200240, China). p33—37

Abstract: The temperature field of electron-beam rapid prototyping is simulated by ANSYS. In this study, heat distribution is expressed as Gaussian equation. The heat loss just includes heat radiation as the process is carried out in the vacuum chamber. Tem-